JOURNAL OF SOLID STATE CHEMISTRY 4, 138–152 (1972)

Magnetic Ordering in $LiCr_{1-x}Fe_xO_2$

A. TAUBER* AND W. M. MOLLER†

Institute for Exploratory Research, U.S. Army Electronics Command, Fort Monmouth, New Jersey 07703

AND

E. BANKS

Department of Chemistry, Polytechnic Institute of Brooklyn, Brooklyn, New York

Received June 10, 1971

Magnetic ordering in the $LiCr_{1-x}Fe_xO_2$ system has been investigated for polycrystal and single crystal specimens characterized by optical and X-ray diffraction techniques. Part of the Li_2O–Fe_2O_3–Cr_2O_3 system was also investigated. Magnetization and susceptibility measurements from 4.2° to 900°K and Mössbauer measurements from 4.2° to 300°K indicate that all compositions of ordered rocksalt (space group $R\bar{3}m$) order antiferromagnetically at low temperatures. The first-order phase transition tracked with all Mössbauer parameters. The Weiss molecular field theory for a layered-type antiferromagnet was fitted with two exchange constants. The dependence of θ on x was found to be

$$\theta = \theta_a(1-x)^2 + \theta_b 2x(1-x) + \theta_c x^2,$$

where $-\theta_a = Cr^{3+}$–Cr^{3+} interaction, $+\theta_b = Fe^{3+}$–Cr^{3+} interaction and $-\theta_c = Fe^{3+}$–Fe^{3+} interaction. A spontaneous magnetization associated with iron-substituted crystals originated with an epitaxial overgrowth of $LiCr_{4.75}Fe_{0.25}O_8$.

Introduction

Compounds with ordered rocksalt structures have been found to exhibit a wide range of magnetic behavior (*1*). Magnetic ordering in compounds of the type $A^{1+}MO_2$, isostructural with $CsCl_2I$ (space group $R\bar{3}m$), where A is an alkali metal and M a transition metal ion, has received little attention.

We have investigated the system $LiCrO_2$–$LiFeO_2$ in which the chromite has the ordered rocksalt structure while the ferrite has the disordered structure. In the disordered form Fe^{3+} and Li^{+1} are randomly distributed over the available octahedral metal sites of the rocksalt structure. If Cr^{3+} is added as a substituent for Fe^{3+}, at first it too occupies the available metal sites statistically. A composition is reached beyond which all metal ions order in alternate metal layers parallel to (111) plane in the cubic phase. The symmetry becomes rhombohedral and, referred to hexagonal axes, the metal layers are perpendicular to the c axis (Fig. 1). The octahedra in the ordered layers continue to share edges as they do in the disordered form.

In the ordered phase all magnetic ions are found in the same metal layers. By virtue of the large interplanar separation (average is 4.8 Å) and the smaller intraplanar separation (average is 2.93 Å) of magnetic ions, a considerable anisotropy in the strength of the magnetic interactions can be expected. Furthermore, the interplanar superexchange path is considerably longer since O–Li–O layers must be traversed. Within the plane the most important interactions expected would be 90° M^{3+}–O–M^{3+} superexchange, 90° direct M^{3+}–M^{3+} exchange, and between planes ~180 superexchange.

We have prepared polycrystalline and single crystal compositions in the system $LiCrO_2$–$LiFeO_2$. Their lattice parameters and Mössbauer spectra

* Abstracted in part from a dissertation to be submitted by Arthur Tauber to the Polytechnic Institute of Brooklyn in partial fulfillment of the requirements for the degree of Doctor of Philosophy in Chemistry.

† Now with Department of Physics, New York University, New York.

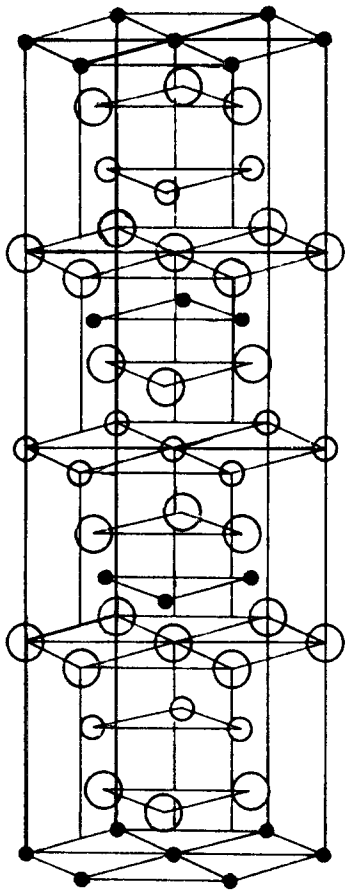

FIG. 1. The crystal structure of $LiCrO_2$ isostructural with $NaCrS_2$ after Rudorff and Stegman [Ref. (*14*)]. Large open circles are O, small open circles are Li, small filled circles, Cr.

have been determined. Magnetic ordering has been investigated in ordered rocksalt compositions by means of magnetization, susceptibility and Mössbauer studies.

The lattice parameters, density and molecular volume in the system $LiCrO_2$–$LiFeO_2$ was prepared and magnetic susceptibility studies were made by Bongers (*3*). Several crystallographic studies have been carried out on trimorphic $LiFeO_2$ (*4–7*). In addition, single crystals (*8*) of this compound have been grown, and have been the subject of Mössbauer (*9*) and susceptibility studies (*10*).

Experimental

Polycrystalline compositions in the system $LiCr_{1-x}Fe_xO_2$ and compositions along the subsolidus $LiFeO_2$–$LiCrO_2$ join (Fig. 2) were prepared from Fisher-certified Li_2CO_3, Fisher-certified Cr_2O_3, and Fe_2O_3 Baker reagent. Corrections were applied for the assayed metal content in formulation. The powdered components were intimately mixed by grinding together in a boron carbide mortar. The mixtures were heated at 700°C for 2 h, reground and reheated at 700°C for up to 4 h in air or CO_2. After grinding, the powders were pressed into 3/32-in. dia cylinders and sealed by welding, in 1/8 in., 0.005-in. wall platinum tubes. These tubes were heated from 24 to 60 h at 1100°C and quenched in air. The cylinders were fractured and examined microscopically for the presence of extraneous phases. X-Ray powder diffractometer patterns were prepared for all samples and again checked for

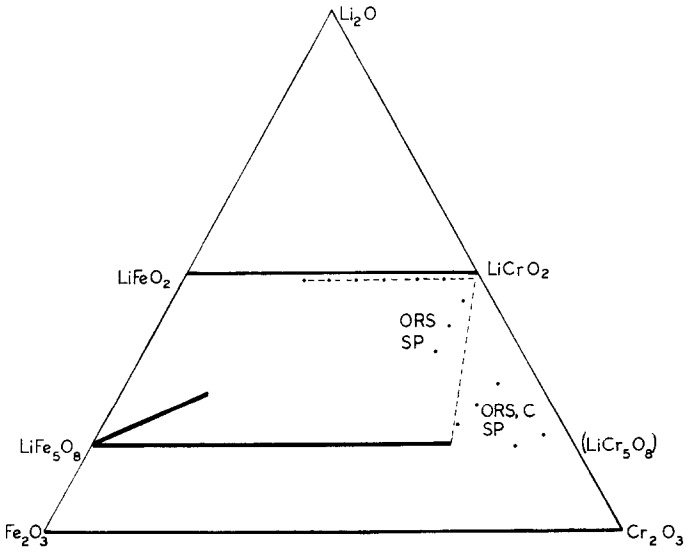

FIG. 2. The system Li_2O–Fe_2O_3–Cr_2O_3: ORS is ordered rocksalt, Sp is spinel, C is corundum.

extraneous phases. In this manner, 1-g samples were prepared and repeated for reproducibility. Two hundred milligrams were set aside each time for susceptibility, magnetization, and Mössbauer studies. The remainder was used to make lattice parameter and intensity measurements.

In addition, compositions in the ternary system Li_2O–Fe_2O_3–Cr_2O_3 poorer in Li_2O than those along the $LiFeO_2$–$LiCrO_2$ subsolidus join were investigated (Fig. 2).

The lattice parameters were obtained for samples along the $LiFeO_2$–$LiCrO_2$ join with the diffractometer data by the method of NBS (*11*) using filtered CuK_α and a pulse height analyzer. Tungsten (99.999% purity) was used as an internal standard. For each composition, an average of values from 00*l* and *hkl* type reflections (for *c*) and *hho*, *hoo* and *hkl* type reflections (for *a*) were employed. Indexing was accomplished by computer fit of the lattice parameters. Preferred orientation is shown by the large value of I_{300}. This precluded the use of powder intensity data for structure analysis.

Crystal Growth

Single crystals of $LiCrO_2$ and $LiCr_{1-x}Fe_xO_2$ were prepared by the flux method in platinum crucibles using lithium borate (*8*). The following compositions and conditions were employed (percentages refer to moles):

(1) 50% Li_2O, 42% B_2O_3, 8% Cr_2O_3 was soaked at a maximum temperature of 1100°C for 20 h and cooled 1.6°C/h to 900°C. All crystals in this investigation were leached with 20% HNO_3 for 1 h. The largest crystals were 0.1-mm thick, green, transparent, hexagonal plates up to 2 mm on an edge. Under the polarizing microscope they were uniaxial negative with very high relief in oil of $n = 1.5$. Color variability due to large dispersion was noted. Red color banding was observed parallel to the basal face. Some crystals, when turned perpendicular to the basal face, showed dichroism; it appeared as if light vibrating parallel to *a* was green, and light vibrating parallel to *c* was red. Precession and Weissenberg patterns using Cu*K* and Mo*K* radiation confirmed $R\bar{3}m$ for the space group.

(2) A composition of 50% Li_2O, 42% B_2O_3, 4% Cr_2O_3 and 4% Fe_2O_3 was soaked for 24 h at a maximum temperature of 1100°C and cooled 2°C/h to 850°C. Crystals were black and had a maximum size of 0.3 mm along octahedral edge. The crystals were determined to be cubic, with spinel-type structure, from powder, rotation, and precession X-ray diffraction diagrams.

(3) A composition of 50% Li_2O, 42% B_2O_3, 7% Cr_2O_3 and 1% Fe_2O_3 was soaked for 24 h at 1125°C and cooled 1.6°C/h to 850°C. The yield was less than 1%. Crystals were red transparent hexagonal plates less than 0.1-mm thick and 1.5-mm maximum size. The space group was determined to be $R\bar{3}m$ from Weissenberg and precession patterns using Cu*K* and Mo*K* radiation. The petrographic microscope showed a uniaxial negative optic figure. Spectrochemical analysis indicated that the iron concentration was less than 0.2% by weight. Mössbauer spectra could not be observed after 10 h at room temperature or 77°K.

TABLE I

INDEXED X-RAY DIFFRACTION POWDER PATTERN OF $LiCrO_2$

h k l	d_{obsd}	d_{calcd}	I/I_o[a]
0 0 3	4.82	4.81	100
1 0 1	2.48	2.48	6
0 0 6	2.405	2.405	3
$\bar{1}$ 0 2 0 1 2	2.368	2.373	2
$\bar{1}$ 1 4 1 0 4	2.061	2.062	14
0 1 5	1.894	1.895	3
0 0 9	1.602	1.603	1
$\bar{1}$ 1 7 1 0 7	1.592	1.593	2
0 1 8	1.465	1.465	4
1 1 0	1.451	1.451	3
$\bar{1}$ 2 3 1 1 3	1.389	1.389	2
$\bar{1}$ 1 1 0 1 0 1 0 0 2 1	1.251	1.251	1
0 0 1 2	1.203	1.202	1
0 2 4	1.185	1.186	1
0 1 1 1 2 0 5 $\bar{2}$ 2 5	1.162	1.163	1
$\bar{1}$ 2 9 1 1 9 0 2 7	1.075	1.075	1
2 0 8	1.031	1.030	1
0 0 1 5	0.9618	0.9618	1
$\bar{2}$ 3 4 2 1 4	0.9182	0.9185	1

[a] I_o is 003.

Magnetic and Mössbauer Data

Magnetization and susceptibility measurements were made from 4.2°K to T_c for crystals with spontaneous magnetization and to about 900°K for susceptibility measurements with a Princeton Applied Research vibrating sample magnetometer. Thermometry between 4.2°K and 300°K was accomplished with a carbon resistor and copper–constantan thermocouple. Above 300°K, a platinum *vs.* platinum 10% rhodium thermocouple was used. The magnetometer was calibrated with nickel (99.999%) [$\sigma = 54.49$ emu/g], $CoSO_4 \cdot 6H_2O$ ($\chi_g = 9300 \times 10^{-6}$ emu/g), $NiSO_4 \cdot 7H_2O$ ($\chi_g = 4300 \times 10^{-6}$ emu/g), and $(NH_4)_2Fe(SO_4)_2 \cdot 6H_2O$ ($\chi_g = 12400 \times 10^{-6}$ emu/g). Where susceptibility data were found to obey a Curie–Weiss law, a least-squares computer fit was employed. Mössbauer studies were carried out with an ICN Tracer Laboratory constant-acceleration, constant-velocity spectrometer model NS-1. Data were collected and stored in a 512 channel Nuclear Data Corp. analyzer. Velocity calibration was accomplished with an annealed ^{57}Fe-enriched soft iron foil and NBS sodium nitroprusside standard. All spectra reported exceeded 10^5 counts/channel, providing a statistical counting error of 0.32 to 0.16%. All spectra were consistently fitted by a Lorentzian least-square computer program. Velocity increments per channel ranged from 0.020 mm/sec to 0.025 mm/sec.

Mössbauer samples were prepared by grinding powders in a boron carbide mortar and passing through a 400-mesh sieve (opening 0.037 mm). Sufficient sample was taken to provide between 10 and 15 mg of iron per cm^2, and mounted rigidly by dispersing with collodion on aluminum foil, mixing with gum arabic and pressing into 2.5-cm diameter discs or mixing with graphite powder and enclosing in a graphite holder. All samples were measured in transmission geometry.

Results and Discussion

Polycrystalline subsolidus compositions investigated are represented by dots in Fig. 2. The rather remarkable complete miscibility of $LiCrO_2$ in $LiFeO_2$, previously reported by Kordes and Petzoldt (*2*), is confirmed. Complete solid solution in a binary system with two end members of different structures is quite rare and occurs because the anion framework differs little between the two structures. The phase diagram represented in Fig. 2 is incomplete. The solid solubility between Cr_2O_3–Fe_2O_3 was described by Wretblad (*12*), $LiFe_5O_8$–$LiCr_5O_8$ by Gorter (*13*) and $LiFeO_2$–$LiCrO_2$, partial $LiFeO_8$–$LiCrO_2$ by Kordes and Petzoldt (*2*). For the region between the two solid solutions, $LiFe_5O_8$–(hypothetical) $LiCr_5O_8$, one expects two phases and indeed this is observed. A three phase region is expected outside a boundary defined by $LiCrO_2$ and the end of the spinel solid solution; this too is found. A solid solution region extending from 45–50 mole % Li_2O parallel to the $LiFeO_2$–$LiCrO_2$ join was found.

In Table I, the computer-calculated *d* spacings are compared with experimental values for $LiCrO_2$. All

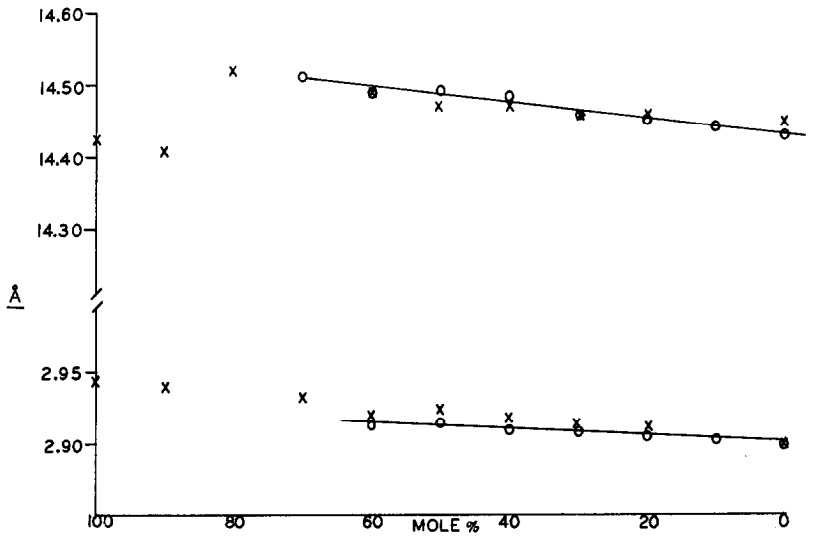

FIG. 3. The variation of lattice parameters with composition in the system $LiFeO_2$–$LiCrO_2$. 100% refers to $LiFeO_2$. The upper curve is for *c*, the lower for *a*.

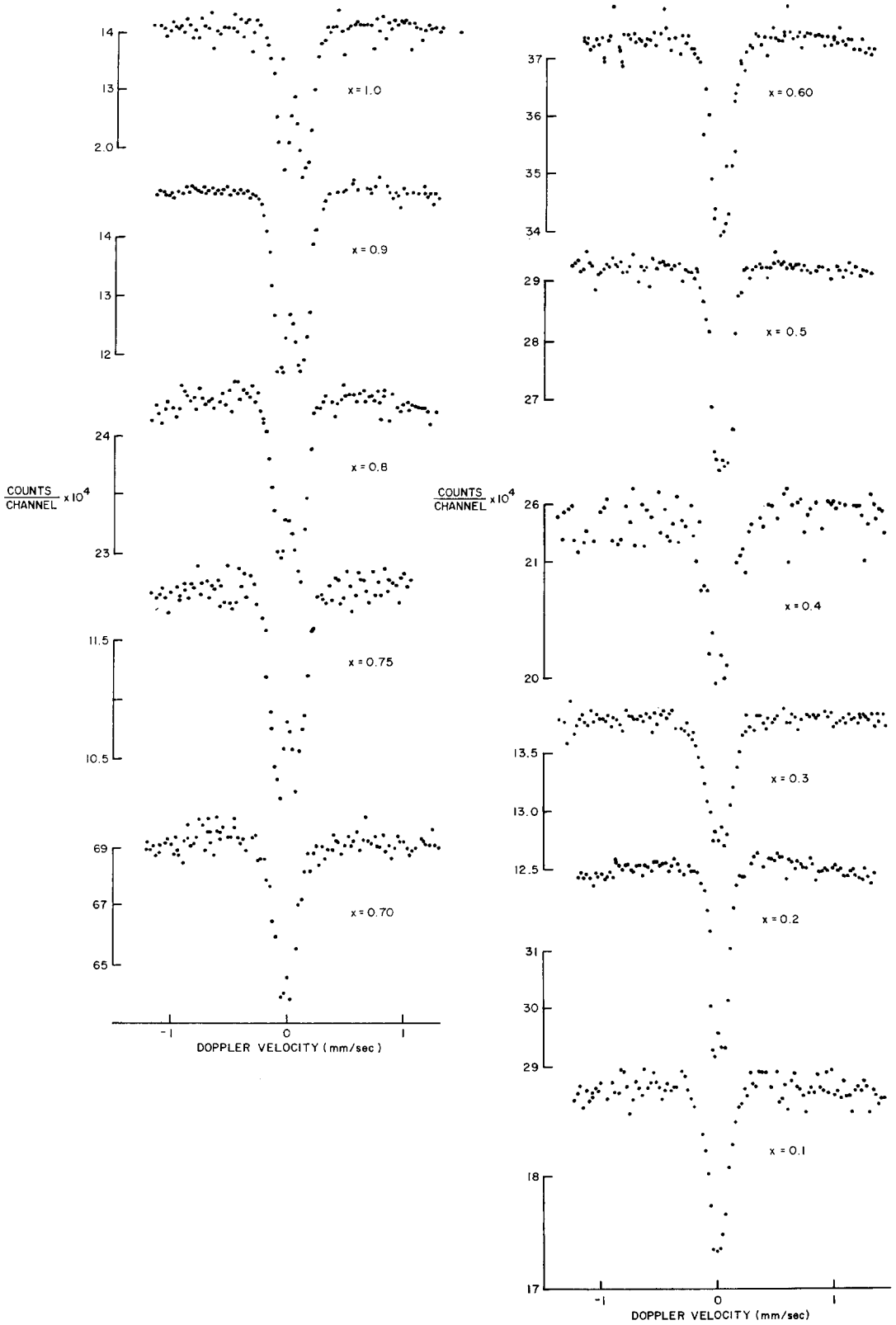

FIG. 4. Mössbauer spectra in the system $LiCr_{1-x}Fe_xO_2$.

ordered rocksalt structures were indexed on this basis. The lattice parameters a and c, referred to a hexagonal cell, are plotted in Fig. 3. The data of this investigation (full circles) are in fair agreement with the earlier work of Kordes and Petzoldt (*2*). However, we find transformation from cubic rocksalt to rhombohedral-ordered rocksalt occurs between 70 and 75 mole % $LiFeO_2$ while Kordes and Petzoldt report the transition between 80 and 90 mole %. Since the latter authors do not mention their quenching rate, it is not now possible to account for this discrepancy.

Mössbauer Spectra

Of the several Mössbauer parameters which may be measured, the quadrupole splitting and hyperfine field are most sensitive to crystal and magnetic ordering. The hyperfine field arises principally from the Fermi contact interaction, which involves the electronic spin density at the nucleus. This spin density is derived from the core s electrons and from s electrons covalently mixed into the open $3d$ shell. The decrease in hyperfine field was initially attributed to covalent reduction of $3d$ spin density at the metal ion site (*17*). More recently, the origin of the covalently reduced hyperfine field has been attributed to the exchange polarization of the bonding orbitals which contain a $4s$ admixture of the metal ion (*19*, *20*).

The Mössbauer parameters were obtained, after subtracting background, by a least-square Lorentzian fit to the spectra of Fig. 4. The $LiFeO_2$ spectrum exhibits a quadrupole split line, first characterized by Cox *et al.* (*9*). These investigators measured 0.50 mm/sec, 0.28 mm/sec and 0.25 mm/sec for the isomer shift, quadrupole splitting, and line width, respectively, employing ^{57}Co diffused in Cu as a source. We employed ^{57}Co diffused in Pt as a source (50 mCi) and noted −0.65 mm/sec for the isomer shift and an FWHM of 0.25 mm/sec on the 20 mg/cm soft iron absorber. Values of 0.026 mm/sec, 0.322 mm/sec, and 0.240 mm/sec were obtained for the isomer shift, quadrupole splitting, and line width of cubic $LiFeO_2$. Referred to iron, the isomer shifts and quadrupole splitting are in excellent agreement. A complete set of Mössbauer spectra are given in Fig. 4. These represent both room-temperature and liquid-nitrogen spectra since both agree within experimental error. This was also observed in $LiFeO_2$ by Cox *et al.* (*9*).

The quadrupole splitting in $LiFeO_2$, although small, is quite distinct. With increasing Cr^{3+}, the amount of splitting diminishes as does the isomer shift and FWHM (Table II). Between $x = 0.75$ and 0.70, a sharp transition is noted. This is seen quite clearly in Fig. 5, and is notable in Table II. The composition $x = 0.70$ is precisely the point of transition from cubic to rhombohedral structure.

In the system $LiCr_{1-x}Fe_xO_2$, one might expect a small increase in the quadrupole splitting when going from cubic to rhombohedral crystal structure. A seemingly anomalous decrease is observed. Cox *et al.* (*9*) suggest that the quadrupole splitting in cubic $LiFeO_2$ is due to a statistical distribution of Li and Fe ions on equivalent sites. Various Fe^{3+} ions may have different numbers of Li^+ ions as nearest and next nearest metal neighbors. This would certainly induce drastic local polarization effects on the oxygen. Viewed in another way, the amount of covalence would drastically change from one iron ion to another. As Cr^{3+} is substituted for Fe^{3+}, a composition is reached beyond which all metal ions order alternately, parallel to [111] in the cubic phase and perpendicular to the c axis in the hexagonal phase (Fig. 1). Thus high local polarization or covalence is diminished, which explains the observed sharp decrease in the quadrupole splitting (*15*, *16*). On the other hand, the effect may be entirely due to the higher local symmetry of the Fe^{3+} ions in the ordered structure.

None of the polycrystalline samples exhibited magnetic ordering above 77°K. The only samples measured near 10°K ($x = 0.6$ and 0.7) exhibited a hyperfine pattern (Fig. 6). Subsequent magnetization and susceptibility measurements demonstrated no spontaneous magnetization (see next section). We have therefore concluded that the manifest ordering

TABLE II

MÖSSBAUER PARAMETERS IN THE SYSTEM $LiCrO_2$–$LiFeO_2$

x	ΔE (mm/sec)	δ^a (mm/sec)	Γ (mm/sec)
1.00	0.322 ± 0.005	0.026 ± 0.005	0.240 ± 0.011
0.90	0.300 ± 0.005	0.026 ± 0.005	0.215 ± 0.007
0.80	0.285 ± 0.006	0.021 ± 0.006	0.225 ± 0.008
0.75	0.286 ± 0.005	0.022 ± 0.005	0.225 ± 0.009
0.70	0.200 ± 0.006	0.014 ± 0.006	0.196 ± 0.008
0.60	0.166 ± 0.006	0.010 ± 0.006	0.158 ± 0.008
0.50	0.158 ± 0.009	0.009 ± 0.009	0.160 ± 0.010
0.40	0.144 ± 0.005	0.006 ± 0.005	0.140 ± 0.007
0.30	0.149 ± 0.005	0.008 ± 0.005	0.148 ± 0.007
0.20	0.141 ± 0.007	0.007 ± 0.007	0.138 ± 0.009
0.10	0.123 ± 0.010	0.002 ± 0.009	0.146 ± 0.011

[a] Referred to platinum source.

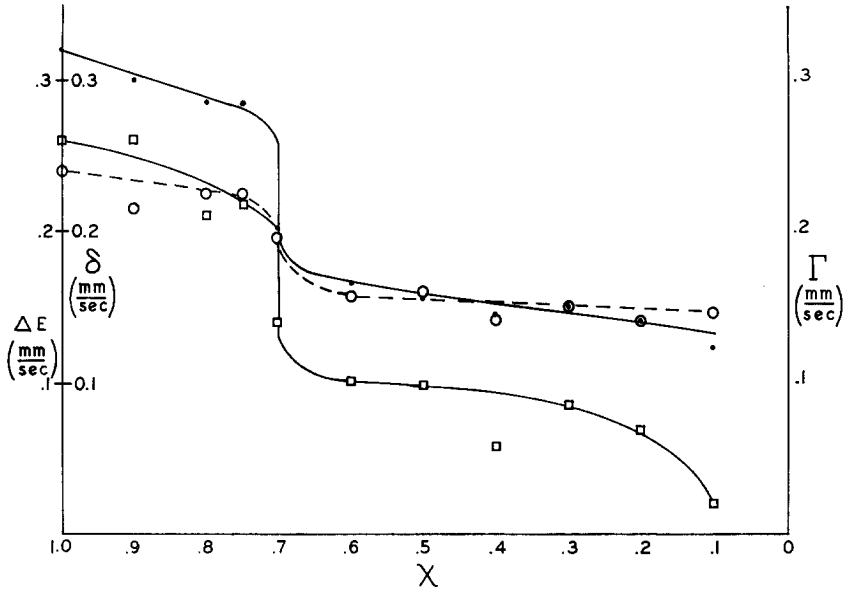

FIG. 5. Mössbauer parameters as a function of composition. Quadrupole splitting, ΔE (dots); isomer shift, δ (boxes); and line width, Γ (circles).

is antiferromagnetic. The parameters for these two compositions are given in Table III. The quadrupole splitting has diminished for both compositions compared with values at 77°K, whereas the isomer shift has increased somewhat (Table II). The internal field was essentially that found in α-Fe_2O_3. In going from $x = 1.0$ to $x = 0.7$ and 0.6, the increase in hyperfine field was noted, consistent with the tendency toward decreased bond polarization (covalence) beyond the cubic–rhombohedral phase transition (*17*, *18*). The

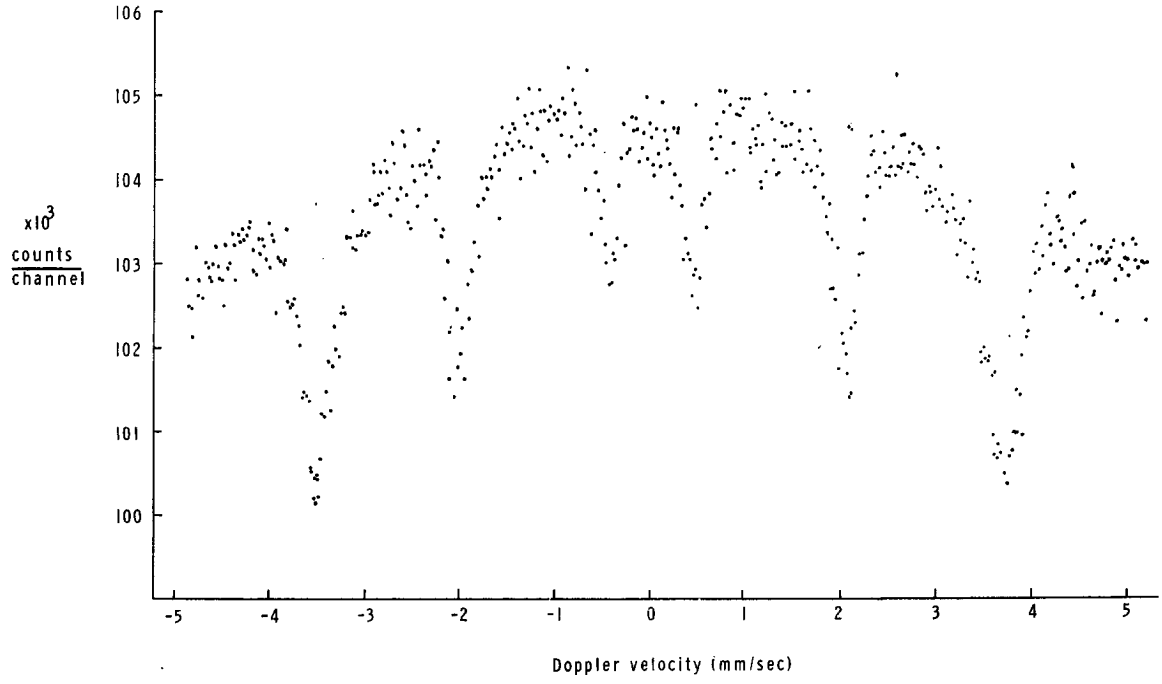

FIG. 6. Hyperfine spectra exhibited by $LiCr_{1-x}Fe_xO_2$ for $x = 0.6$ and 0.7 at 10°K.

TABLE III

MÖSSBAUER HYPERFINE DATA

Composition	δ (mm/sec)	ΔE (mm/sec)	H_n (kOe)	Γ_{ave} (mm/sec)
$x = 1.0$	0.100 ± 0.03	0.28 ± 0.03	495 (at 4.2°K)[a]	0.15
$x = 0.7$	0.083 ± 0.03	0.054 ± 0.03	510	0.133
$x = 0.6$	0.063 ± 0.05	0.014 ± 0.05	515	0.25
α-Fe_2O_3	−0.350		515 (at 300°K)	

[a] References (*9*) and (*14*).

increase in lattice parameters on ordering is additional evidence for decreasing covalency. This may be a result of every transition metal ion having lithium neighbors in adjacent layers, so that the interlayer bonding is more ionic.

Susceptibility

The susceptibility was measured on polycrystalline ordered compositions ($x = 0$ to $x = 0.7$) in fields up to 15 kOe. The variation of the inverse molar susceptibility as a function of temperature is given in Figs. 7–12. Bongers (*3*) has previously measured $LiCrO_2$ on polycrystalline materials. We have essentially reproduced his results between 4.2 and 300°K. However, we did not note a minimum in the $1/\chi$ *vs.* T plot (Fig. 5) and could not confirm his approximate value of 200°K for T_n. Our magnetometer was not sufficiently sensitive to measure the largest single crystals (wt 1 mg). We therefore loaded our sample holder with about one hundred crystals so that their c axes (referred to hexagonal system) were perpendicular to the applied field. The single crystal curve of Fig. 5(b) was thus obtained. The susceptibility obeys a Curie–Weiss law above 450°K. A least-squares fit to the data gives a paramagnetic Curie point, $\theta = -570$°K. The magnetic moment of 3.55 ± 0.11 μB is in fair agreement with 3.71 μB obtained by Bongers (*3*); his θ value, −577°K, differs by only 7°K. Below 250°K, the curve changes slope and declines sharply until 12°K, below which the curve is approximately flat to 4.2°K. This temperature-independent behavior suggests that the Cr spins are aligned parallel to c; this is opposite to the orientation found in isostructural $NaCrSe_2$ and $NaCrS_2$ (*21*).

Polycrystalline samples with varying x exhibit similar magnetic behavior. A Curie–Weiss law was

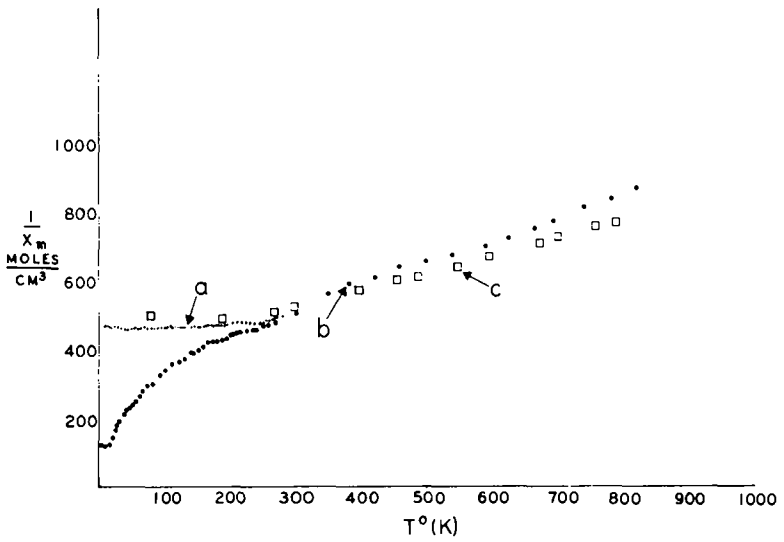

FIG. 7. The inverse molar susceptibility dependence on temperature for $LiCrO_2$. Large dots (b) are single crystals H ⊥ C, small dots (a) are polycrystalline, open squares (c) are data of P. F. Bongers (*3*).

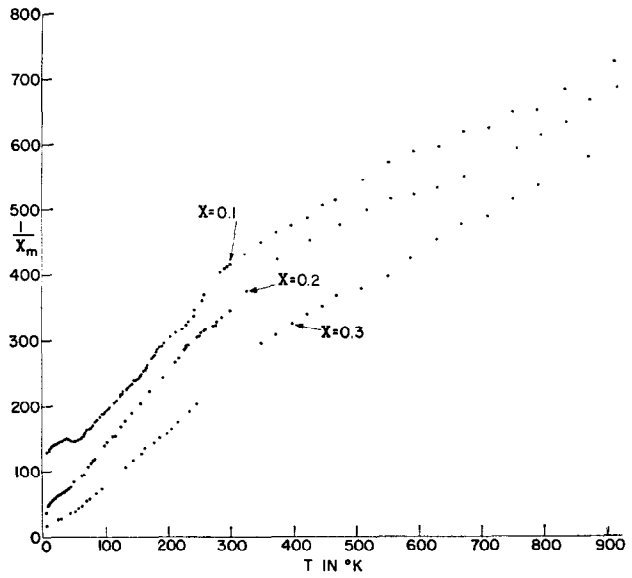

FIG. 8. The inverse molar susceptibility dependence on temperature in the system $LiCr_{1-x}Fe_xO_2$, $x = 0.1$, 0.2, and 0.3.

computer-fitted to the data of $x = 0.1$, 0.2 and 0.3 above 600°K, and $x = 0.4$, 0.5, 0.6, and 0.7 above 400°K. The $x = 0.1$ composition shows a minimum near 50°K, while the curves for the other compositions exhibit a change in slope in the 40–55°K temperature range.

The parameters obtained from the fit to a Curie–Weiss law are given in Table IV. The magnetic moments are compared with summed spin-only values, which show a reduction with increasing x. This reduction is midway between values expected for high spin (given in Table IV) and low spin for Fe^{3+}. We do not believe that this is due to a change in the distribution of high-spin and low-spin Fe^{3+}. It may be a consequence of the anisotropic magnetic coupling in the ordered state. This could be checked by comparing ordered and disordered samples of the same composition. Since our samples were quenched from 1100°C, this experiment would entail either more rapid quenching or quenching from higher temperatures. Attempts will be made to obtain such samples in the future.

The paramagnetic Curie points are plotted in Fig. 13; a parabolic quadratic variation is suggested. The decrease in the large negative θ values to zero with increasing x suggests the introduction of ferro-

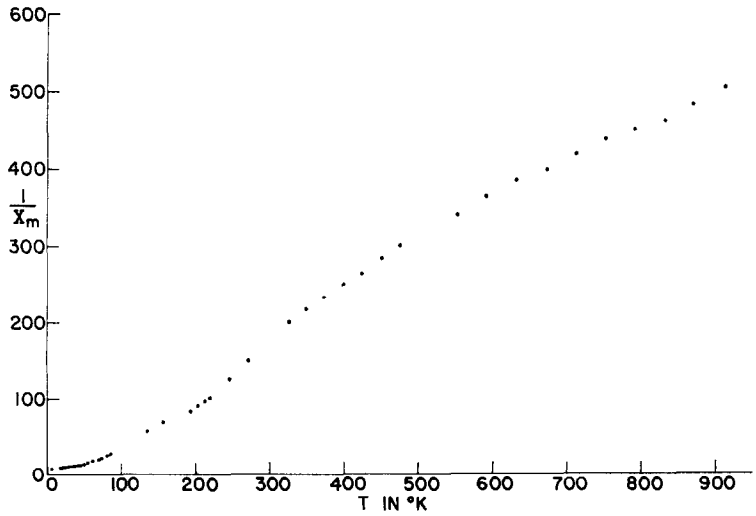

FIG. 9. Inverse molar susceptibility dependence on temperature for $LiCr_{0.40}Fe_{0.6}O_2$.

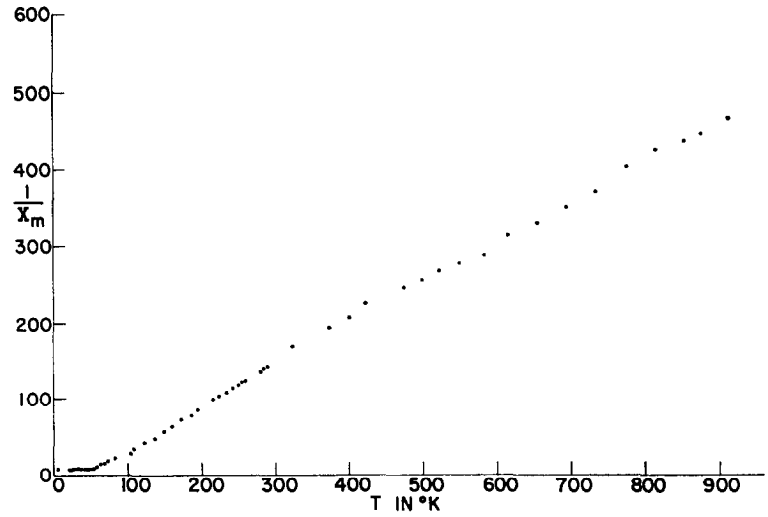

FIG. 10. Inverse molar susceptibility dependence on temperature for $LiCr_{0.5}Fe_{0.5}O_2$.

magnetic exchange. This must be due to Fe^{3+}–O–Cr^{3+} intraplanar 90° exchange, since the ordered rocksalt is a cubic close-packed structure with transition metal intraplanar layers separated by 4.8 Å with intervening O–Li–O layers. Actual exchange path length is in excess of this distance. Three-dimensional antiferromagnetic ordering through two oxygens or two oxygens and a diamagnetic Rh^{3+} or Al^{3+} ion has been discussed by Blasse (*22*) and Roth (*23*) in spinels. They demonstrate superexchange through these intervening ions, but with Néel temperatures not exceeding 40°K. We have taken, as an indicator of antiferromagnetic ordering and T_n, the sudden change of slope at temperatures $\leqslant$55°K. The departure from Curie–Weiss behavior for a considerable temperature range above T_n suggests the onset of two-dimensional ordering much above the three-dimensional antiferromagnetic ordering temperature.

In the following treatment, the Weiss molecular field model was employed to estimate the strength of intralayer J_1 and interlayer J_2 exchange interactions. The HDV Hamiltonian, following Smart (*24*), for a single atom with two types of interactions is

$$H = -2J_1 S_i \cdot \sum_{j=1}^{z} S_j - 2J_2 S_i \cdot \sum_{j=1}^{z} S_j,$$

where the summation is carried out over nearest neighbors of the ith atom. For layer lattice type 1, Smart has computed a set of equations relating θ,

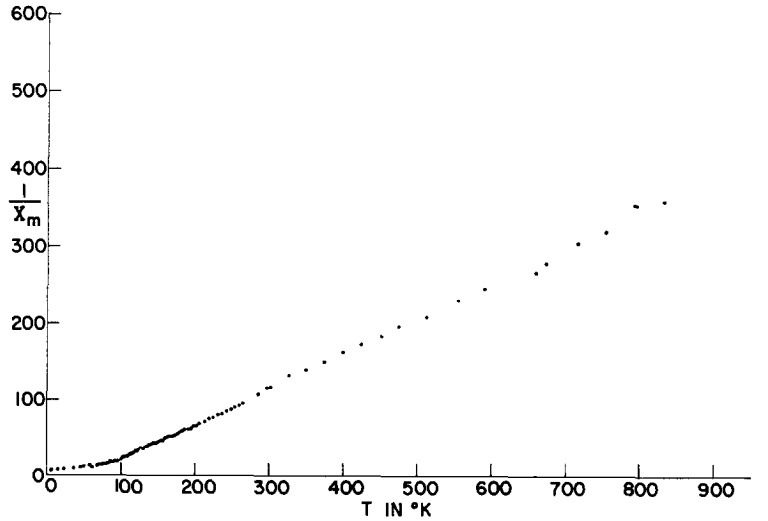

FIG. 11. Inverse molar susceptibility dependence on temperature for $LiCr_{0.6}Fe_{0.4}O_2$.

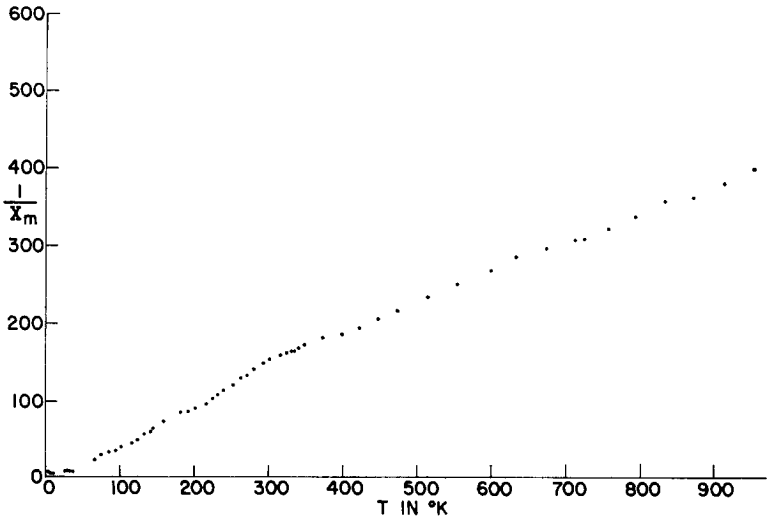

FIG. 12. Inverse molar susceptibility dependence on temperature for $LiCr_{0.7}Fe_{0.3}O_2$.

T_n and $X_{(T_n)}$ (*25*). Because there is considerable uncertainty in T_n, the best method of estimating J_2 is from the susceptibility $X_{(T_n)}$ at the Néel temperature:

$$Cm/X_{(T_n)} = 8J_2\,S(S+1)/k.$$

With the exception of $x = 0.1$ and 0.2 where small minima were observed in the $1/\chi_m$ *vs.* temperature plots, T_n was taken as the break in slope of $1/\chi_m$ at very low temperatures. The susceptibility at and below this point changes very slowly with temperature.

Since θ is equal to the sum of all exchange interactions

$$\theta = \theta_1 + \theta_2 = [2/3S(S+1)]\,[6J_1/k + 6J_2/k],$$

where

$$\theta_1 = 2/3S(S+1)\,6J_1/k, \quad \theta_2 = 2/3S(S+1)\,6J_2/k.$$

Values of J_1/k, J_2/k, θ_1 and θ_2 are given in Table IV.

The quadratic variation in θ with x, already noted, is reflected in θ_1 and θ_2 variations with x. Jonker (*26*) has previously shown that such behavior in perovskites originates in the various probabilities of interaction for two different magnetic species. In $LiCr_{1-x}Fe_xO_2$, we define the exchange interactions:

$\theta_a = Cr^{3+}$–Cr^{3+} interaction,
fraction of neighbors $= (1-x)^2$

$\theta_b = Cr^{3+}$–Fe^{3+} interaction,
fraction of neighbors $= 2x(1-x)$

$\theta_c = Fe^{3+}$–Fe^{3+} interaction,
fraction of neighbors $= x^2$

then, $\theta_1 = \theta_a(1-x)^2 + \theta_b 2x(1-x) + \theta_c x^2$. This quadratic is a parabola, consistent with the observa-

TABLE IV

MAGNETIC PARAMETERS

x	C_m (cm^3 °K/M)	μB (exptl)	μB[a] (calcd)	θ (°K)	θ_1 (°K)	θ_2 (°K)	T_n (approx) (°K)	J_1/K (°K)	J_2/K (°K)
0	1.58	3.57	3.87	−570	−472	−98	15	−33	−6.9
0.1	1.98	4.17	4.07	−546	−399	−147	56	−25	−8.5
0.2	1.76	3.77	4.28	−300	−180	−120	40	−17	−4.3
0.3	1.90	3.91	4.49	−204	−138	−66	35	−11	−2.2
0.4	1.81	3.83	4.69	−25	+7.5	−32.5	50	−0.70	−1.1
0.5	1.82	3.83	4.90	0	+16.3	−16.3	55	+0.58	−0.6
0.6	2.40	4.39	5.10	−47	−35.5	−11.5	45	−1.8	−0.7
0.7	2.64	4.65	5.30	−94	−80.5	−13	40	−3.7	−0.6

[a] Spin only, high spin.

tions of Fig. 13. It is assumed that θ_a, θ_b, and θ_c are constants over the composition range investigated.

The constants are computed in two ways: Thirty-five simultaneous equations were solved in determinantal form by computer program and averaged. The data were also analyzed by regression analysis with a computer program. The fit for specific points is shown in Fig. 14. The coefficient of determination r^2 was 0.943 for θ. The final constants were obtained by averaging the results of both analyses: For θ_1,

$$\theta_a = -625°\text{K}, \text{Cr}^{3+}\text{–Cr}^{3+}; \quad \theta_b = +708°\text{K}, \text{Fe}^{3+}\text{–Cr}^{3+};$$
$$\theta_c = -726°\text{K}, \text{Fe}^{3+}\text{–Fe}^{3+}.$$

The signs are consistent with the Goodenough–Kanamori rules (*27*, *28*) for 90° superexchange.

For d^3–d^5, Goodenough (*27*) distinguished six possible types of 90° superexchange. Of these the following should make contributions: (1) delocalized antiferromagnetic cation–cation via half filled t_{2g} orbitals, (2) delocalized antiferromagnetic $Cr^{3+}t_{2g}$ to $Fe^{3+}e_g$ transfer, and (3) delocalized ferromagnetic $Fe^{3+}t_{2g}$ to $Cr^{3+}e_g$ transfer; (4) antiferromagnetic correlation superexchange simultaneously via $O^{2-}p_x$ and p_y transfer to $Fe^{3+}e_g$ and $Cr^{3+}e_g$; (5) ferromagnetic correlation superexchange via simultaneous $O^{2-}2s$ transfer to $Fe^{3+}e_g$ and $Cr^{3+}e_g$. Delocalization superexchange e_g–e_g interaction does not occur because the oxygen p_x and p_y orbitals are orthogonal to each other. For the Fe^{3+}–Cr^{3+} ferromagnetic superexchange, surprisingly, dominates over antiferromagnetic.

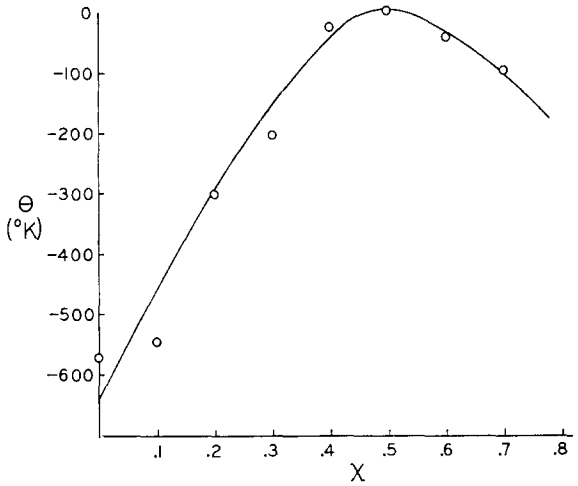

FIG. 13. Dependence of paramagnetic Curie point upon x.

A similar analysis may be applied to θ_2 for interplanar superexchange: For θ_2,

$$\theta_{2a} = -185°\text{K}, \text{Cr}^{3+}\text{–Cr}^{3+};$$
$$\theta_{2b} = +59°\text{K}, \text{Fe}^{3+}\text{–Cr}^{3+};$$
$$\theta_{2c} = -30°\text{K}, \text{Fe}^{3+}\text{–Fe}^{3+}.$$

The r^2 was 0.975 for θ_2. The positive Fe^{3+}–Cr^{3+} is clearly predicted as the most probable type for 180° Fe^{3+}–Cr^{3+} superexchange (*26*, *27*). Contributions to J_2 are quite small.

A small spontaneous magnetization (σ_s) was found in the Fe^{3+}-doped $LiCrO_2$ crystals described

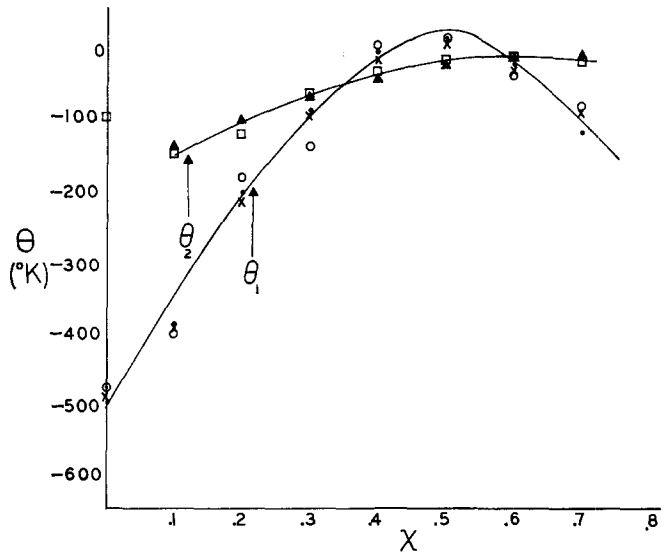

FIG. 14. Computer fit to θ_1 and θ_2 dependence on x. For θ_1, circles are experimental, crosses are fit by regression analysis, dots are fit by determinants. For θ_2, triangles are experimental, boxes are fit by regression analysis.

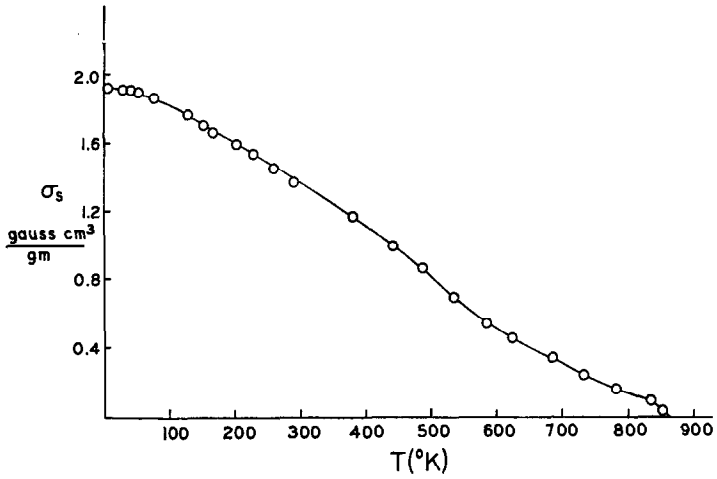

FIG. 15. Spontaneous magnetization as a function of temperature in Fe^{3+}-doped $LiCrO_2$.

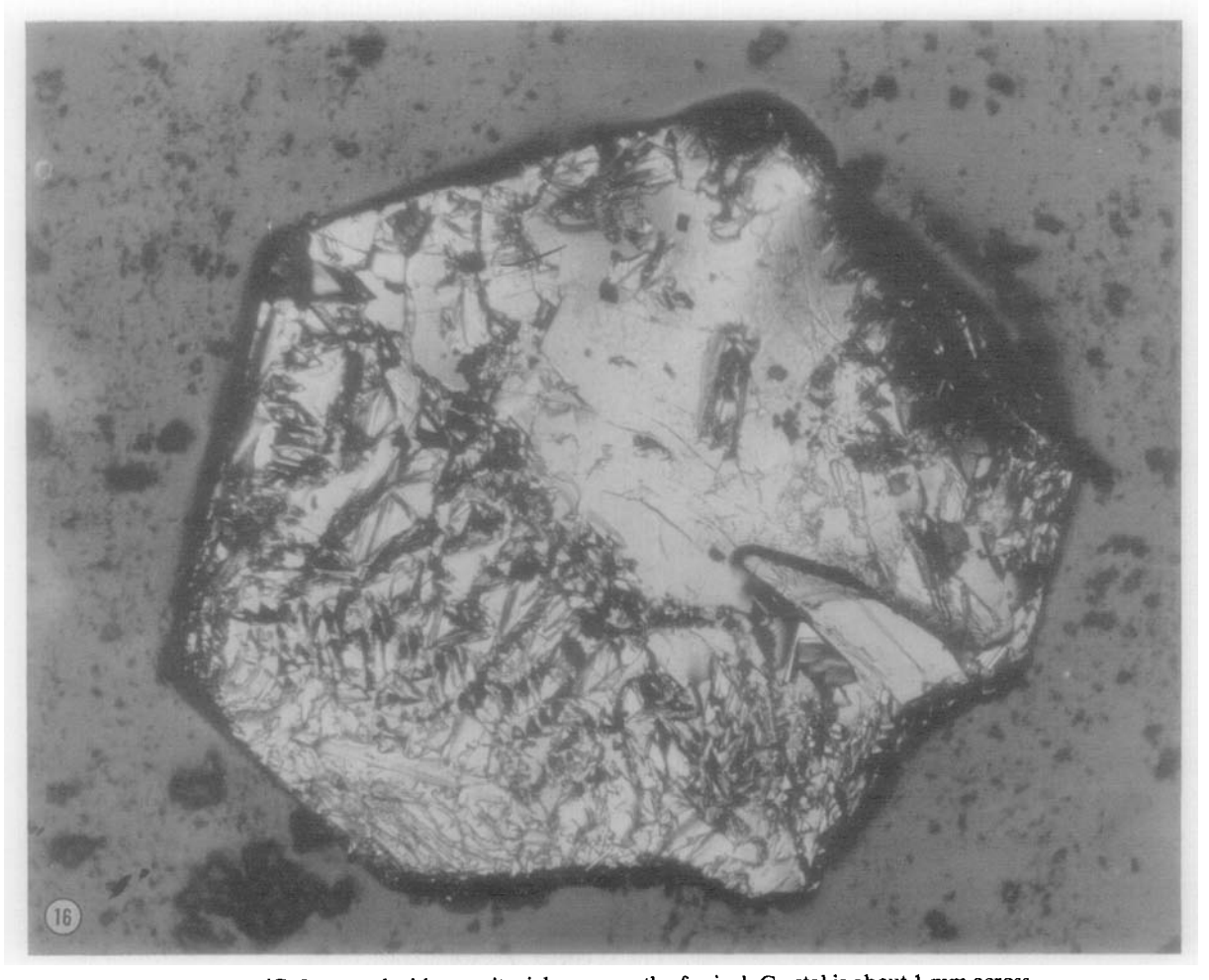

FIG. 16. $LiCrO_2$ crystal with an epitaxial overgrowth of spinel. Crystal is about 1-mm across.

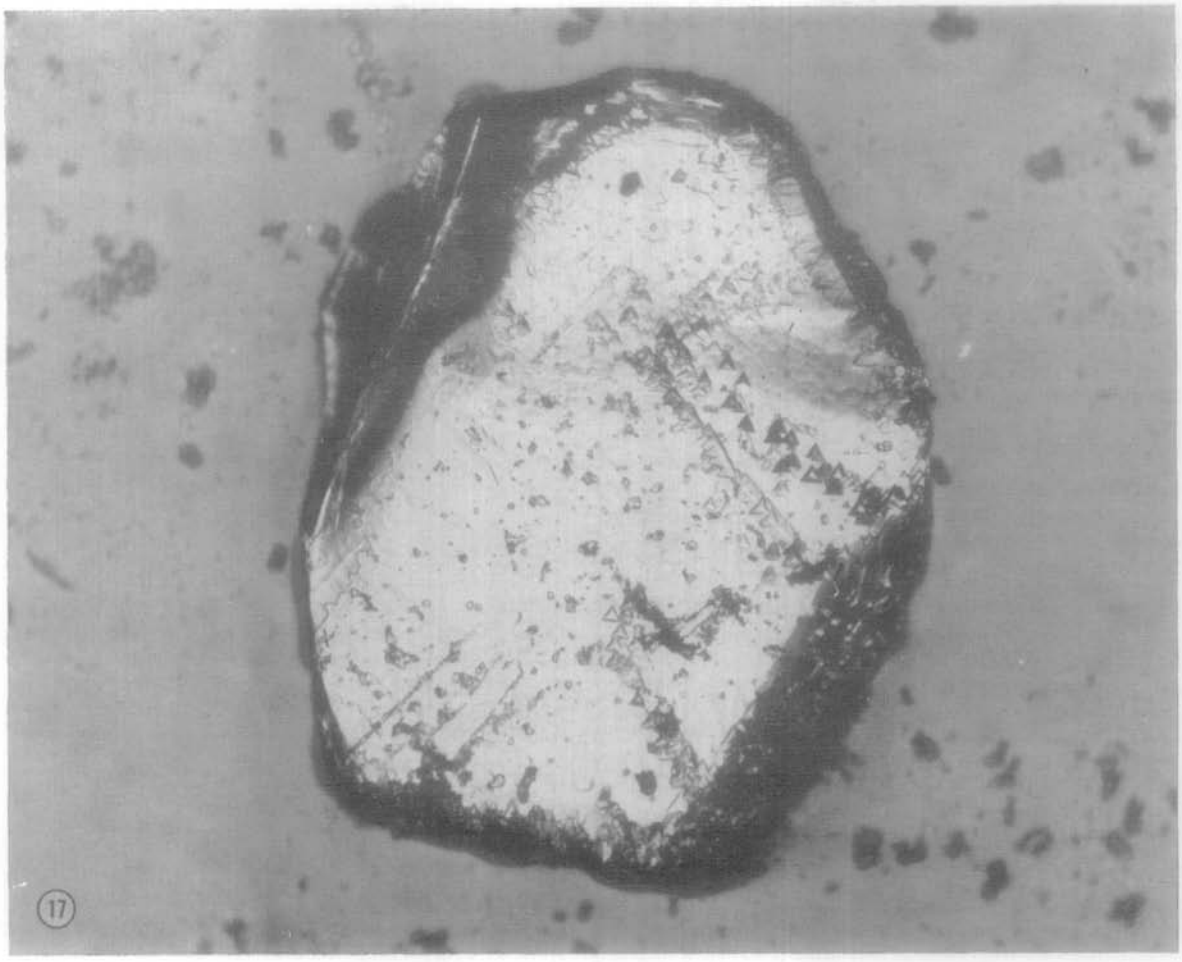

FIG. 17. Crystal of $LiCrO_2$ after treatment with H_2SO_4.

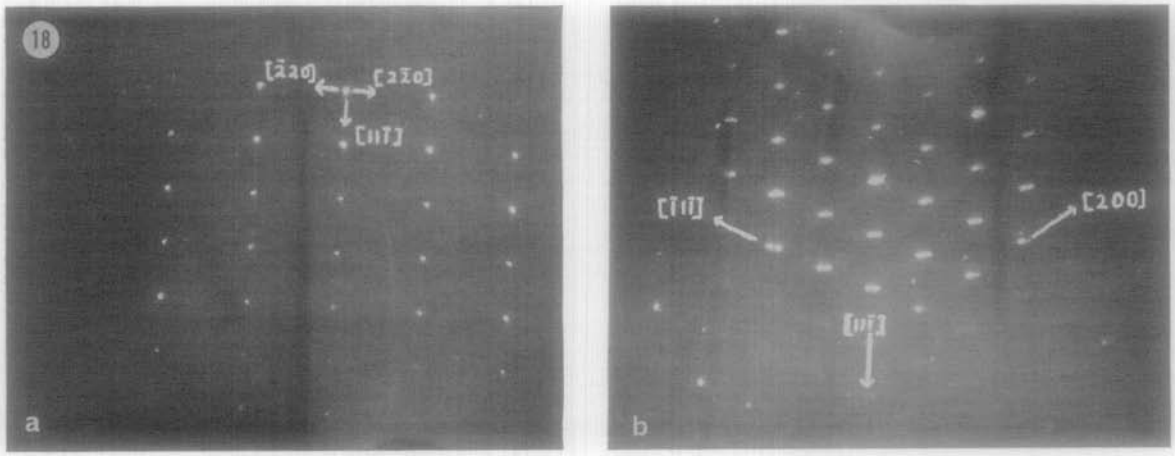

FIG. 18. Reciprocal lattice pattern of spinel obtained by reflection diffraction with the main beam parallel to [$\bar{2}$24] in *a* and [0$\bar{2}\bar{2}$] in *b*.

above, under "Crystal Growth". Figure 15 is a plot of σ_s *vs.* T in °K. The magnetization curves obey a $\sigma = \sigma_s + xH$ law similar to those described by Anderson *et al.* (*10*). Since the crystals were transparent to light, they were examined under the polarizing microscope. When rotated between crossed Nicols parallel to the *c* axis, only isotropic behavior could be found. However, in reflected light, an oriented overgrowth was found (Fig. 16). HCl did not remove this deposit. Boiling in H_2SO_4 for 5 min removed the overgrowth and etched the crystal, as shown in Fig. 17. Furthermore, the spontaneous magnetization disappeared, supporting the conclusion that it was not intrinsic, but due most probably to spinel overgrowth of the type $LiFe_{5-x}Cr_xO_8$. The Curie point T_c was determined by Belov's method (*29*). The value of $T_c = 805$°K corresponds to $x = 0.25$ as deduced from Gorter's data (*13*). Reflection electron diffraction patterns of etched and unetched crystals confirmed the presence of spinel. The nets were indexed with $a_0 = 8.32$ Å. In Fig. 18, the single crystal diffraction pattern labeled "a" was obtained with main beam parallel to $[\bar{2}24]$, and "b" with the main beam parallel to $[\overline{022}]$ on the single crystal spinel overgrowth.

Acknowledgments

The authors are grateful to O. Berkooz and J. Deluca (Polytechnic Institute of Brooklyn) for Mössbauer measurements near the temperature of liquid helium; to J. R. Shappirio, C. F. Cook, and W. F. Nye (ECOM, Fort Monmouth, N.J.) for microprobe, interference microscopy and electron microscopy and diffraction analysis of many samples; and to J. S. Megill and M. Grebenau (ECOM, Fort Monmouth, N.J.) for assistance in magnetic measurements.

References

1. D. G. Wickham, *Rec. Chem. Progr.* **27**, 59 (1966).
2. E. Kordes and J. Petzoldt, *Z. Anorg. Allg. Chem.* **335**, 138 (1965).
3. P. F. Bongers, Dissertation, p. 44, University of Leiden, Leiden, Netherlands, 1957.
4. M. Brunel and F. De Bergevin, *J. Phys. Chem. Solids* **29**, 163 (1968).
5. E. C. Collongues, *C.R. Acad. Sci. Paris* **241**, 1577 (1955).
6. M. Fayard, *Ann. Chim.* **6**, 1279 (1961).
7. J. C. Anderson and M. Schieber, *J. Phys. Chem. Solids* **25**, 961 (1964).
8. J. C. Anderson and M. Schieber, *J. Phys. Chem. Solids* **25**, 1838 (1964).
9. D. E. Cox, G. Shirane, P. A. Flinn, S. L. Ruby, and W. J. Takei, *Phys. Rev.* **132**, 1547 (1963).
10. J. C. Anderson, S. K. Dey, and V. Halpern, *J. Phys. Chem. Solids* **26**, 1555 (1965).
11. H. E. Swanson, M. C. Morris, and E. H. Evans, "Standard X-Ray Diffraction Powder Patterns," NBS Monograph 25, Sec. 4, U.S. Gov't. Printing Office, Washington 25, D.C. 1966.
12. P. E. Wretblad, *Z. Anorg. Allg. Chem.* **189**, 544 (1930).
13. E. W. Gorter, *Philips Res. Rep.* **9**, 403 (1954).
14. W. Rudorff and K. Stegman, *Z. Anorg. Allg. Chem.* **251**, 376 (1943).
15. J. Danon, *J. Chem. Phys.* **39**, 136 (1963).
16. J. Danon, "Chemical Application of Mössbauer Spectroscopy," Chap. 3, p. 224, Academic Press, New York, 1968.
17. J. S. Van Wieringen, *Discuss. Faraday Soc.* **119**, 118 (1955).
18. O. Matumura, *J. Phys. Soc. Jap.* **14**, 108 (1959).
19. J. C. M. Henning, *Phys. Lett. A* **24**, 40 (1967).
20. E. S. Simanek and K. A. Muller, *J. Phys. Chem. Solids* **31**, 1027 (1970).
21. P. F. Bongers, C. F. Van Bruggen, J. Koopstra, W. P. F. A. M. Orloo, G. A. Wiegers, F. Jellinek, *J. Phys. Chem. Solids* **29**, 977 (1968).
22. G. Blasse, *Philips Res. Rep.* **18**, 383 (1963).
23. W. L. Roth, *J. Phys. Paris* **25**, 507 (1964).
24. J. S. Smart, "Effective Field Theories of Magnetism," Chap. 1, p. 24, W. B. Saunders Co., Philadelphia, PA, 1966.
25. J. S. Smart, "Magnetism" (G. T. Rado and H. Suhl, eds.), Vol. III, Chap. 2, p. 111, Academic Press, New York, 1963.
26. G. H. Jonker, *Physica* **22**, 707 (1956).
27. J. B. Goodenough, "Magnetism and the Chemical Bond," p. 180, Interscience, New York, 1963.
28. J. Kanamori, *J. Phys. Chem. Solids* **10**, 87 (1959).
29. K. P. Belov, "Magnetic Transitions," Chap. 3, p. 34, Consultants Bureau Enterprises, New York, 1961.